




## Article

# VUV Pump and Probe of Phase Separation and Oxygen Interstitials in $\text{La}_2\text{NiO}_{4+y}$ Using Spectromicroscopy

Antonio Bianconi <sup>1,2,3,4,\*</sup> , Augusto Marcelli <sup>1,5</sup> , Markus Bendele <sup>1</sup>, Davide Innocenti <sup>6</sup>, Alexei Barinov <sup>7</sup>, Nathalie Poirot <sup>8</sup> and Gaetano Campi <sup>2,\*</sup> 

<sup>1</sup> Rome International Center of Materials Science Superstripes, RICMASS, Via dei Sabelli 119A, 00185 Rome, Italy; augusto.marcelli@inf.infn.it (A.M.); markus.bendele@gmail.com (M.B.)

<sup>2</sup> Institute of Crystallography, Consiglio Nazionale delle Ricerche, IC-CNR, Via Salaria Km 29.300, Monterotondo, I-00015 Rome, Italy

<sup>3</sup> National Research Nuclear University, MEPhI (Moscow Engineering Physics Institute), Kashirskoye sh. 31, 115409 Moscow, Russia

<sup>4</sup> Latvia Academy of Science, Akadēmijas laukums 1, LV-1050 Riga, Latvia

<sup>5</sup> Laboratori Nazionali di Frascati, Istituto Nazionale di Fisica Nucleare, 00044 Frascati, Italy

<sup>6</sup> Department of Chemistry, University of Liverpool, Liverpool L69 7ZD, UK; davide.innocenti@liverpool.ac.uk

<sup>7</sup> Sincrotrone Trieste S.C.p.A., Area Science Park, 34012 Basovizza, Italy; alexey.barinov@elettra.eu

<sup>8</sup> Institut Universitaire de Technologie de Blois (IUT Blois), Université de Tours, 15, Rue de la Chocolaterie, 41029 Blois, France; nathalie.poirot@univ-tours.fr

\* Correspondence: antonio.bianconi@ricmass.eu (A.B.); gaetano.campi@ic.cnr.it (G.C.)

Received: 17 January 2018; Accepted: 9 February 2018; Published: 11 February 2018

**Abstract:** While it is known that strongly correlated transition metal oxides described by a multi-band Hubbard model show microscopic multiscale phase separation, little is known about the possibility to manipulate them with vacuum ultraviolet (VUV), 27 eV lighting. We have investigated the photo-induced effects of VUV light illumination of a super-oxygenated  $\text{La}_2\text{NiO}_{4+y}$  single crystal by means of scanning photoelectron microscopy. VUV light exposure induces the increase of the density of states (DOS) in the binding energy range around  $E_b = 1.4$  eV below  $E_F$ . The photo-induced states in this energy region have been predicted due to clustering of oxygen interstitials by band structure calculations for large supercell of  $\text{La}_2\text{CuO}_{4.125}$ . We finally show that it is possible to generate and manipulate oxygen rich domains by VUV illumination as it was reported for X-ray illumination of  $\text{La}_2\text{CuO}_{4+y}$ . This phenomenology is assigned to oxygen-interstitials ordering and clustering by photo-illumination forming segregated domains in the  $\text{La}_2\text{NiO}_{4+y}$  surface.

**Keywords:** defects in multi-band Hubbard model; photo-induced effects; oxygen interstitials; phase separation; quasi stationary states out of equilibrium; metastable phases; defects self-organization

## 1. Introduction

Writing patterns in organic and inorganic media by illumination, starting from silver-halide processes for traditional photography, is a key method to manipulate materials for advanced technologies. In the last decade, photo-induced effects have been investigated in the families of strongly correlated complex quantum matter like transition metal oxides, showing high temperature superconductivity [1–14] and colossal magneto resistance [15,16]. Controlling photo-induced effects in complex matter is of high interest in nanotechnology for novel oxide nanoelectronics on demand [17–21]. The interest has been mostly addressed on  $(\text{A}_2\text{MO}_{4+y})$  systems having the  $\text{K}_2\text{NiF}_4$ -type structure with  $\text{A} = \text{Cu}$ , i.e.,  $\text{La}_2\text{CuO}_{4+y}$  structure, which received much attention since these compounds show

nano-scale phase separation [22–24]. The emergence of multiscale phase separation from nano-scale to micron-scale has been explained to be driven by tuning the chemical potential at a Lifshitz transition in a multi-band Hubbard model [25–27]. In this regime, the competition between spin, charge, orbital and elastic interactions can drive the system into metastable phases, i.e., quasi stationary states out of equilibrium with the coexistence and competition between a metallic phase and a localized charge ordered phase. While “large polarons” spanning about 8 lattice sites in the intermediate coupling regime have been found in cuprates, [28] “small polarons” localized in a single lattice unit cell in the strong coupling regime have been found in manganites [29]. In these systems a relevant lattice effect is due to mobile oxygen interstitials in the spacer layers, which contribute to the complexity with the formation of dopant rich domains anticorrelated with charge ordered domains which control the nanoelectronic functionality [30].

In these complex systems characterized by a large variety of coexisting superconducting, insulating, ferromagnetic, antiferromagnetic states, X-ray illumination induces electronic and structural changes [1–21] allowing tuning of material functionalities, which allow the development of many device capabilities. The electronic properties of super-oxygenated  $\text{La}_2\text{NiO}_{4+y}$  have high technological interest [31–39]. This  $\text{A}_2\text{MO}_{4+y}$  system  $\text{A} = \text{Ni}$  having the  $\text{K}_2\text{NiF}_4$ -type structure has the ability to accommodate a large oxygen over-stoichiometry. It is formed by a stack of bcc atomic  $\text{NiO}_2$  layers intercalated by  $[\text{La}_2\text{O}_{2+y}]$  atomic layers similar to the simplest high temperature cuprate superconductor  $\text{La}_2\text{CuO}_{4+y}$ , but it does not show superconductivity at any measurable doping level. It may be possible that oxygen interstitial ordering at room temperature can be manipulated in  $\text{La}_2\text{NiO}_{4+y}$  as in the cuprate  $\text{La}_2\text{CuO}_{4+y}$ .

The  $[\text{NiO}_2]$  layers are typical charge transfer Mott insulators [31–39]. The  $\text{Ni}^{2+}$  ion has a  $\text{Ni } 3d^8$  configuration whereas the antiferromagnetic order is comparable to  $\text{NiO}$ . The mobile oxygen interstitials in  $\text{La}_2\text{NiO}_{4+y}$  enter in the rocksalt spacer layer  $[\text{La}_2\text{O}_{2+y}]$  and sit at  $(1/4, 1/4, 1/4)$  type positions of the orthorhombic lattice creating  $nh = 2y$  holes into the  $\text{NiO}_2$  planes. The doped holes enter in the oxygen 2p orbital L forming  $3d^8L$  localized states, similar to  $\text{NiO}$  [40]. The  $3d^8L$  states form “small polarons” localized on single atomic oxygen L sites in the  $\text{NiO}_2$  plane where the doped charge is associated with a local lattice distortion of the  $\text{NiO}_2$  plane similarly to the insulating phase of manganites [29]. The idea of polaron ordering in doped  $\text{NiO}_2$ , as the source of magnetic stripes driven by doping, has been proposed by Zaanen and Littlewood [33]. In doped Mott–Hubbard insulators, the electron-phonon interaction and the strong Coulomb repulsion can reinforce each other to stabilize small polarons, domain walls, and charge-density waves. At low temperature, the holes are ordered such that they form polaronic stripes of localized charges and magnetic moments in the diagonal direction of the Ni–O bond direction. The complexity of the striped magnetic phase is related to phase separation and ordering of oxygen interstitials. Measurements of the in-plane resistance in the nickelates suggest that oxygen interstitial orderings appear below  $T_{\text{CO}} = 320$  K. In comparison, the magnetic and small polaron ordering occurs at temperature lower than  $T_m = 110$  K.

The ordering of oxygen interstitials in the  $\text{CuO}_2$  plane in the families of cuprates is controlled by the compressive misfit strain [41,42] in the  $[\text{CuO}_2]$  active layer near the spacer layer  $[\text{La}_2\text{O}_{2+y}]$ . The  $[\text{CuO}_2]$  compressive strain is compensated by the  $[\text{La}_2\text{O}_{2+y}]$  tensile misfit strain in the formation of the multilayer crystal. The increase of the  $[\text{CuO}_2]$  compressive misfit strain pushes the system to the formation of small polarons, but at the same time the  $[\text{La}_2\text{O}_{2+y}]$  tensile misfit strain determines the increase of the mobility of the  $y$  oxygen interstitials. This is the case of doped  $\text{La}_2\text{NiO}_{4+y}$  where, due to the large tensile misfit strain in the  $[\text{La}_2\text{O}_{2+y}]$ , the mobility of oxygen interstitials is high. The latter is in fact an oxygen ion conductor at high temperature with high technological relevance [43–50]. Synchrotron radiation investigations of  $\text{La}_2\text{NiO}_{4+y}$  [51,52] and  $\text{La}_2\text{CuO}_{4+y}$  [53] have been performed using standard XANES, X-ray absorption near edge structure, [54–58] interpreted considering many body final states configurations, relevant in these strongly correlated oxides [59–65].

## 2. Results and Discussion

Scanning photoelectron microscopy (SPEM) was performed on the insulating  $\text{La}_2\text{NiO}_{4+y}$  ( $y = 0.14$ ) [34,35,66]. The SPEM measurements were performed at the SPECTROMICROSCOPY-3.2L beamline at the Elettra synchrotron light source, Trieste (Italy) [67,68]. Data presented here were collected at the photon energy of 27 eV. The beam size in focus is  $\sim 500$  nm FWHM by a Schwarzschild objective. The VUV illumination was performed by leaving sample under same but defocused beam having donut like shape due to a presence of central stop in the optics. Surface effects such as topographical contrast were eliminated by following the procedure described in [67].

Energy distribution curves of selected micro-spots of illuminated and non-illuminated regions are presented in Figure 1. A clear difference between these photoelectron spectra has been observed. In the light exposed regions an increase of the DOS compared to the non-illuminated DOS can be observed. The difference of the DOS between illuminated and non-illuminated photoelectron spectra is represented by the blue curve in Figure 1. It reveals that states in the region around 1.4 eV below  $E_F$  are those affected by light illumination. Actually, photons in the VUV region with an energy  $h\nu = 27$  eV lead to a significant change of the DOS in  $\text{La}_2\text{NiO}_{4+y}$ . This result is in excellent agreement with the theoretical simulations of the increase of ordered oxygen interstitial domains presented in Figure 2 that suggest that the DOS increases in this energy region due to oxygen interstitials.

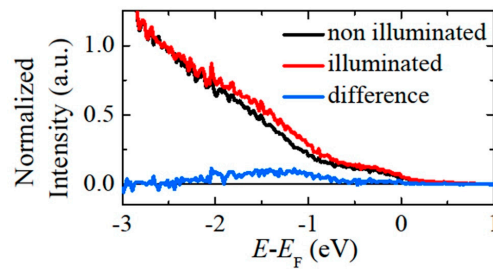


**Figure 1.** The density of states (DOS) of the  $\text{La}_2\text{NiO}_{4+y}$  below the Fermi level  $E_F$  before (black line, non-illuminated) and after light illumination (red line, illuminated) measured by vacuum ultraviolet (VUV) photoemission using an incident photon beam of 27 eV. A clear increase of the DOS is seen in the binding energy  $E_b = E - E_F$  range centered around  $E_b = 1.4$  eV, illustrated by the difference curve (blue line).

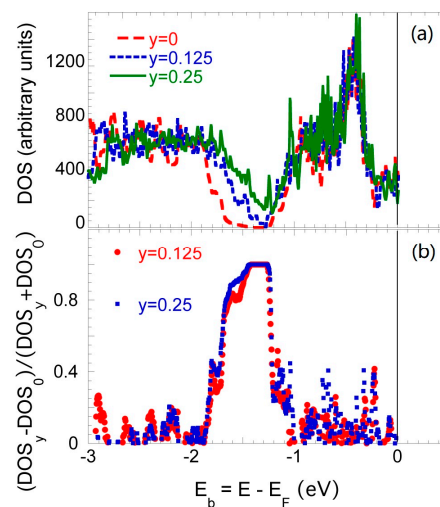


**Figure 2.** (a) Total DOS for  $\text{La}_2\text{NiO}_{4+y}$  for different oxygen interstitials concentrations  $y = 0, 0.125$  and  $0.25$  and (b) the relative increase of the DOS centered at 1.4 eV binding energy the for  $y = 0.25$  and  $y = 0.125$  oxygen interstitial concentration relative to the undoped lattice ( $y = 0$ , from [69]).

Detailed simulations on the variation of the electronic band structure vs. oxygen interstitials concentration were performed by Jarlborg et al. [69–71] using the linear muffin-tin orbital method and the local spin density approximation. These simulations on  $\text{La}_2\text{CuO}_{4+y}$  are in good agreement with experimental results. The excess oxygen interstitials sit at the interstitial interlayer positions, above the oxygen ion in the  $\text{CuO}_2$  plane of the orthorhombic unit cell, form 3D ordered puddles below 320 K. The non-magnetic total band DOSs for  $n = 0, 1$  and  $2$  corresponding to  $y = 0, y = 0.125$  and  $y = 0.25$  are displayed in Figure 2a. It can be seen that the DOS is increasing considerably near  $E_F$  when one or two Oi's are added in form of stripes, as also shown by the relative increase of the DOS in Figure 2b.

In the imaging mode, the analyzer channels well below the Fermi energy  $E_F$  can be used to detect surface effects whereas others above  $E_F$  are used to determine the background. This allows determining differences in the electronic structure and to spatially resolve the averaged spectroscopic information from photoemission.

In Figure 3a a SPEM image is shown where photoelectrons are collected around normal to the sample surface. The intensity, from white to black, represents the photoemission spectroscopy yield integrated over the binding energies around 1.4 eV below  $E_F$ . The DOS in this binding energy range appears homogeneous over the sample surface with no significant visible features. The corresponding histogram of the normalized integrated intensity in an energy window of 0.6 eV around 1.4 eV below  $E_F$  is shown in Figure 3b. This Gauss like distribution points that the DOS at every point of the surface is the same.

The illuminated region in the SPEM image shown in Figure 3c is represented as a bright broken circle. In this region, the DOS in the energy window of 0.6 eV around 1.4 eV below  $E_F$  is higher than in the non-illuminated regions. This is demonstrated by the shape of the histogram shown in Figure 3d that exhibits a double peak structure. The maximum of the main peak is nearly at the same integrated normalized intensity as the non-illuminated contribution shown in Figure 3b, characteristic of the signal from the non-illuminated area of the sample. The second maximum in Figure 3d occurs at a significantly higher integrated intensity, representing the average intensity after the illumination.

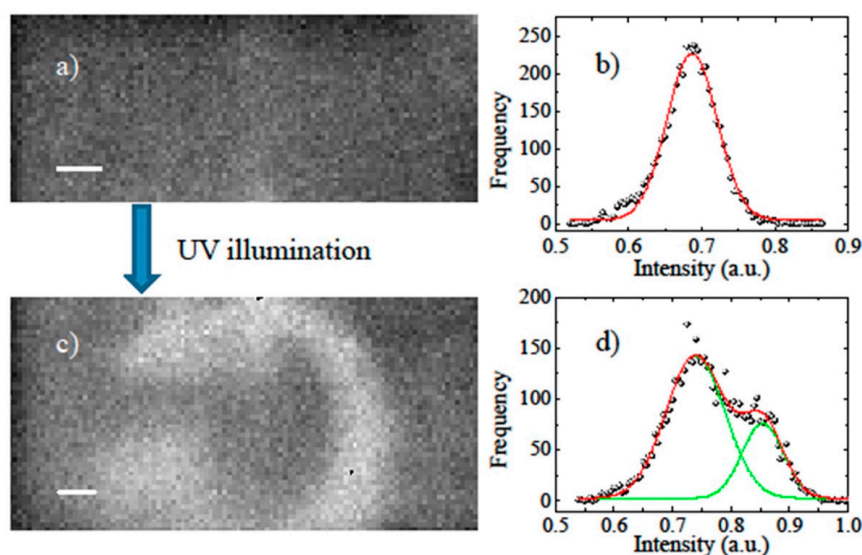


**Figure 3.** (a) Scanning photoelectron microscopy (SPEM) image of  $\text{La}_2\text{NiO}_{4+y}$  of a non-illuminated region with no inhomogeneity; (b) the corresponding histogram shows a homogeneous distribution of the integrated intensity with the Gauss shape; (c) SPEM image after the illumination with the defocused beam with photons of 27 eV. Where the  $\text{La}_2\text{NiO}_{4+y}$  sample was exposed to the light, an increase of the integrated intensity is observed. This is also seen in the corresponding histogram; (d) after the illumination two maxima are present representing the low-intensity non-illuminated area of the sample and the illuminated area with higher intensity. The scale bar in panel (a,c) corresponds to 10  $\mu\text{m}$ .

### 3. Conclusions

In conclusion, scanning photoelectron microscopy measurements of valence band photoemission were performed in order to measure the effect of photon illumination on super-oxygenated  $\text{La}_2\text{NiO}_{4+y}$  ( $y = 0.14$ ). The light exposure leads to an increase of the DOS mainly in the region around 1.4 eV below  $E_F$ , in agreement with calculations showing an increase of the DOS in the same energy window, due to oxygen interstitials. An effect of light illumination was observed by several other experiments as well. Scanning nano X-ray diffraction studies on  $\text{La}_2\text{CuO}_{4+y}$  revealed that light exposure in super-oxygenated LCO lead to an ordering of the oxygen interstitials forming rows in the  $\text{La}_2\text{CuO}_{4+y}$ , the spacer  $\text{La}_2\text{O}_2$  layer between the active layers [9–11]. Such induced ordering can be used to induce new states in transition metal oxides, supporting the development of new device possibilities. Finally, this experiment shows that spectromicroscopy can be successfully used to pump and probe photoinduced mechanisms in complex solids and biological matter in quasi-stationary states out-of-equilibrium [72–76].

**Acknowledgments:** The authors thank ELETTRA, synchrotron radiation facility at Trieste, Italy for the beam time and the SPECTROMICROSCOPY-3.2L beamline staff for support.

**Author Contributions:** A.B., M.B. and G.C. conceived and designed the experiment; N.P. provided and characterized the single crystals; M.B. and D.I. performed the experiments; A.B., M.B. and G.C. analyzed the data; A.B., A.M. and G.C. wrote the paper. All authors have read and approved the final manuscript.

**Conflicts of Interest:** The authors declare no conflict of interest.

### References

1. Nieva, G.; Osquiguil, E.; Guimpel, J.; Maenhoudt, M.; Wuyts, B.; Bruynseraede, Y.; Maple, M.B.; Schuller, I.K. Photoinduced enhancement of superconductivity. *Appl. Phys. Lett.* **1992**, *60*, 2159–2161. [[CrossRef](#)]
2. Kudinov, V.I.; Chaplygin, I.L.; Kirilyuk, A.I.; Kreines, N.M.; Laiho, R.; Lähderanta, E.; Ayache, C. Persistent photoconductivity in  $\text{YBa}_2\text{Cu}_3\text{O}_{6+x}$  films as a method of photodoping toward metallic and superconducting phases. *Phys. Rev. B* **1993**, *47*, 9017–9028. [[CrossRef](#)]
3. Lederman, D.; Hasen, J.; Schuller, I.K.; Osquiguil, E.; Bruynseraede, Y. Photoinduced superconductivity and structural changes in high temperature superconducting films. *Appl. Phys. Lett.* **1994**, *64*, 652–654. [[CrossRef](#)]
4. Bianconi, G.; Di Castro, D.; Saini, N.L.; Bianconi, A.; Colapietro, M.; Pifferi, A. Charge stripes formation by X-ray illumination in high  $T_c$  superconductors. *AIP Conf. Proc.* **2000**, *506*, 358–371.
5. Campi, G.; Castro, D.D.; Bianconi, G.; Agrestini, S.; Saini, N.L.; Oyanagi, H.; Bianconi, A. Photo-Induced phase transition to a striped polaron crystal in cuprates. *Phase Transit.* **2002**, *75*, 927–933. [[CrossRef](#)]
6. Campi, G.; Di Castro, D.; Dell’omo, C.; Agrestini, S.; Saini, N.L.; Bianconi, A.; Bianconi, G.; Barba, L.; Cassetta, A.; Colapietro, M. Temperature and X-Ray illumination effects in oxygen doped  $\text{La}_2\text{CuO}_4$ . *Int. J. Mod. Phys. B* **2003**, *17*, 836–841. [[CrossRef](#)]
7. Campi, G.; Dell’omo, C.; Di Castro, D.; Agrestini, S.; Filippi, M.; Bianconi, G.; Barba, L.; Cassetta, A.; Colapietro, M.; Saini, N.L.; et al. Effect of temperature and X-ray illumination on the oxygen ordering in  $\text{La}_2\text{CuO}_{4.1}$  superconductor. *J. Supercond.* **2004**, *17*, 137–142. [[CrossRef](#)]
8. Fratini, M.; Campi, G.; Simonelli, L.; Palmisano, V.; Agrestini, S.; Filippi, M.; Saini, N.; Bianconi, A. Activation energy of the photo induced  $q_2$  oxygen ordered phase in the  $\text{La}_2\text{CuO}_{4.08}$  superconductor. *J. Supercond.* **2005**, *18*, 71–74. [[CrossRef](#)]
9. Fratini, M.; Campi, G.; Barba, L.; Busby, Y.; Filippi, M.; Prellier, W.; Palmisano, V.; Simonelli, L.; Saini, N.; Bianconi, A. Manipulation of mesoscopic phase separation by X-ray illumination. *J. Supercond. Nov. Magn.* **2007**, *20*, 551–554. [[CrossRef](#)]
10. Poccia, N.; Fratini, M.; Ricci, A.; Campi, G.; Barba, L.; Vittorini-Orgeas, A.; Bianconi, G.; Aeppli, G.; Bianconi, A. Evolution and control of oxygen order in a cuprate superconductor. *Nat. Mater.* **2011**, *10*, 733–736. [[CrossRef](#)] [[PubMed](#)]
11. Poccia, N.; Bianconi, A.; Campi, G.; Fratini, M.; Ricci, A. Size evolution of the oxygen interstitial nanowires in  $\text{La}_2\text{CuO}_{4+y}$  by thermal treatments and X-ray continuous illumination. *Supercond. Sci. Technol.* **2012**, *25*, 124004. [[CrossRef](#)]



12. Pagliero, A.; Mino, L.; Borfecchia, E.; Truccato, M.; Agostino, A.; Pascale, L.; Enrico, E.; Leo, N.D.; Lamberti, C.; Martínez-Criado, G. Doping change in the Bi-2212 superconductor directly induced by a hard X-ray nanobeam. *Nano Lett.* **2014**, *14*, 1583–1589. [[CrossRef](#)] [[PubMed](#)]
13. Truccato, M.; Agostino, A.; Borfecchia, E.; Mino, L.; Cara, E.; Pagliero, A.; Adhlakha, N.; Pascale, L.; Operti, L.; Enrico, E.; et al. Direct-Write X-ray nanopatterning: A proof of concept Josephson device on  $\text{Bi}_2\text{Sr}_2\text{CaCu}_2\text{O}_{8+\delta}$  superconducting oxide. *Nano Lett.* **2016**, *16*, 1669–1674. [[CrossRef](#)] [[PubMed](#)]
14. Campi, G.; Ricci, A.; Poccia, N.; Fratini, M.; Bianconi, A. X-rays Writing/Reading of charge density waves in the  $\text{CuO}_2$  plane of a simple cuprate superconductor. *Condens. Matter* **2017**, *2*, 26. [[CrossRef](#)]
15. Kiryukhin, V.; Casa, D.; Hill, J.P.; Keimer, B.; Vigliante, A.; Tomioka, Y.; Tokura, Y. An X-ray-induced insulator—Metal transition in a magnetoresistive manganite. *Nature* **1997**, *386*, 813–815. [[CrossRef](#)]
16. Lai, K.; Nakamura, M.; Kundhikanjana, W.; Kawasaki, M.; Tokura, Y.; Kelly, M.A.; Shen, Z.X. Mesoscopic percolating resistance network in a strained manganite thin film. *Science* **2010**, *329*, 190–193. [[CrossRef](#)] [[PubMed](#)]
17. Soh, Y.-A.; Aeppli, G.; Zimmermann, F.M.; Isaacs, E.D.; Frenkel, A.I. X-ray induced persistent photoconductivity in Si-doped  $\text{Al}_{0.35}\text{Ga}_{0.65}\text{As}$ . *J. Appl. Phys.* **2001**, *90*, 6172–6176. [[CrossRef](#)]
18. Caviglia, A.D.; Gariglio, S.; Reyren, N.; Jaccard, D.; Schneider, T.; Gabay, M.; Thiel, S.; Hammerl, G.; Mannhart, J.; Triscone, J.M. Electric field control of the  $\text{LaAlO}_3/\text{SrTiO}_3$  interface ground state. *Nature* **2008**, *456*, 624–627. [[CrossRef](#)] [[PubMed](#)]
19. Cen, C.; Thiel, S.; Mannhart, J.; Levy, J. Oxide nanoelectronics on demand. *Science* **2009**, *323*, 1026–1030. [[CrossRef](#)] [[PubMed](#)]
20. Cavalleri, A.; Chong, H.H.W.; Fourmaux, S.; Glover, T.E.; Heimann, P.A.; Kieffer, J.C.; Mun, B.S.; Padmore, H.A.; Schoenlein, R.W. Picosecond soft X-ray absorption measurement of the photoinduced insulator-to-metal transition in  $\text{VO}_2$ . *Phys. Rev. B* **2015**, *69*, 153106. [[CrossRef](#)]
21. Bischak, C.G.; Hetherington, C.L.; Wu, H.; Aloni, S.; Oglethorpe, D.F.; Limmer, D.T.; Ginsberg, N.S. Origin of reversible photoinduced phase separation in hybrid perovskites. *Nano Lett.* **2017**, *17*, 1028–1033. [[CrossRef](#)] [[PubMed](#)]
22. Dabrowski, B.; Jorgensen, J.D.; Hinks, D.G.; Pei, S.; Richards, D.R.; Vanfleet, H.B.; Decker, D.L.  $\text{La}_2\text{CuO}_{4+y}$  and  $\text{La}_2\text{NiO}_{4+y}$ : Phase separation resulting from excess oxygen defects. *Phys. C Supercond.* **1989**, *162*–164, 99–100. [[CrossRef](#)]
23. Fratini, M.; Poccia, N.; Ricci, A.; Campi, G.; Burghammer, M.; Aeppli, G.; Bianconi, A. Scale-free structural organization of oxygen interstitials in  $\text{La}_2\text{CuO}_{4+y}$ . *Nature* **2010**, *466*, 841–844. [[CrossRef](#)] [[PubMed](#)]
24. Poccia, N.; Ricci, A.; Campi, G.; Fratini, M.; Puri, A.; Di Gioacchino, D.; Marcelli, A.; Reynolds, M.; Burghammer, M.; Saini, N.L.; et al. Optimum inhomogeneity of local lattice distortions in  $\text{La}_2\text{CuO}_{4+y}$ . *Proc. Natl. Acad. Sci. USA* **2012**, *109*, 15685–15690. [[CrossRef](#)] [[PubMed](#)]
25. Kugel, K.I.; Rakhmanov, A.L.; Sboychakov, A.O.; Poccia, N.; Bianconi, A. Model for phase separation controlled by doping and the internal chemical pressure in different cuprate superconductors. *Phys. Rev. B* **2008**, *78*, 165124. [[CrossRef](#)]
26. Bianconi, A.; Poccia, N.; Sboychakov, A.O.; Rakhmanov, A.L.; Kugel, K.I. Intrinsic arrested nanoscale phase separation near a topological lifshitz transition in strongly correlated two-band metals. *Supercond. Sci. Technol.* **2015**, *28*, 024005. [[CrossRef](#)]
27. Bianconi, A. Lifshitz transitions in multi-band Hubbard models for topological superconductivity in complex quantum matter. *J. Supercond. Nov. Magn.* **2017**. [[CrossRef](#)]
28. Bianconi, A.; Messori, M. The instability of a 2D electron gas near the critical density for a Wigner polaron crystal giving the quantum state of cuprate superconductors. *Solid State Commun.* **1994**, *91*, 287–293. [[CrossRef](#)]
29. Lanzara, A.; Saini, N.L.; Brunelli, M.; Natali, F.; Bianconi, A.; Radaelli, P.G.; Cheong, S.-W. Crossover from Large to Small Polarons across the Metal-Insulator Transition in Manganites. *Phys. Rev. Lett.* **1998**, *81*, 878–881. [[CrossRef](#)]
30. Littlewood, P. Superconductivity: An X-ray oxygen regulator. *Nat. Mater.* **2011**, *10*, 726–727. [[CrossRef](#)] [[PubMed](#)]
31. Goodenough, J.B.; Ramasesha, S. Further evidence for the coexistence of localized and itinerant 3d electrons in  $\text{La}_2\text{NiO}_4$ . *Mater. Res. Bull.* **1982**, *17*, 383–390. [[CrossRef](#)]

32. Aeppli, G.; Buttrey, D.J. Magnetic correlations in  $\text{La}_2\text{NiO}_{4+\delta}$ . *Phys. Rev. Lett.* **1988**, *61*, 203–206. [[CrossRef](#)] [[PubMed](#)]
33. Zaanen, J.; Littlewood, P.B. Freezing electronic correlations by polaronic instabilities in doped  $\text{La}_2\text{NiO}_4$ . *Phys. Rev. B* **1994**, *50*, 7222–7225. [[CrossRef](#)]
34. Poirrot-Reveau, N.; Odier, P.; Simon, P.; Gervais, F. Signature of stripes in the optical conductivity of  $\text{La}_2\text{NiO}_{4.11}$ . *Phys. Rev. B* **2002**, *65*, 094503. [[CrossRef](#)]
35. Poirrot, N.; Gervais, F. Analysis of temperature dependence of electrical conductivity in  $\text{La}_2\text{NiO}_{4.14}$  single crystal. *J. Supercond. Nov. Magn.* **2005**, *18*, 749–752. [[CrossRef](#)]
36. Poirrot, N.; Phuoc, V.T.; Gruener, G.; Gervais, F. Dependence of optical conductivity with  $\delta$  in  $\text{La}_2\text{NiO}_{4+\delta}$  single crystals. *Solid State Sci.* **2005**, *7*, 1157–1162. [[CrossRef](#)]
37. Poirrot, N.; Simon, P.; Odier, P. Anomalies of ESR spectra of the  $\text{La}_2\text{NiO}_{4+\delta}$  system. *Solid State Sci.* **2008**, *10*, 186–192. [[CrossRef](#)]
38. Poirrot, N.; Souza, R.A.; Smith, C.M. Evidences of stripe charge and spin ordering in  $\text{La}_2\text{NiO}_{4+\delta}$  by electron spin resonance. *Solid State Sci.* **2011**, *13*, 1494–1499. [[CrossRef](#)]
39. Abu-Shiekah, I.M.; Bakharev, O.; Brom, H.B.; Zaanen, J. First time determination of the microscopic structure of a stripe phase: Low temperature NMR in  $\text{La}_2\text{NiO}_{4.17}$ . *Phys. Rev. Lett.* **2001**, *87*, 237201. [[CrossRef](#)] [[PubMed](#)]
40. Davoli, I.; Marcelli, A.; Bianconi, A.; Tomellini, M.; Fanfoni, M. Multielectron configurations in the X-ray-absorption near-edge structure of NiO at the oxygen K threshold. *Phys. Rev. B* **1986**, *33*, 2979–2982. [[CrossRef](#)]
41. Di Castro, D.; Bianconi, G.; Colapietro, M.; Pifferi, A.; Saini, N.L.; Agrestini, S.; Bianconi, A. Evidence for the strain critical point in high  $T_c$  superconductors. *Eur. Phys. J. B* **2000**, *18*, 617–624. [[CrossRef](#)]
42. Bianconi, A.; Agrestini, S.; Bianconi, G.; Di Castro, D.; Saini, N.L. A quantum phase transition driven by the electron lattice interaction gives high  $T_c$  superconductivity. *J. Alloys Compd.* **2001**, *317–318*, 537–541. [[CrossRef](#)]
43. Skinner, S.J.; Kilner, J.A. Oxygen ion conductors. *Mater. Today* **2003**, *6*, 30–37. [[CrossRef](#)]
44. Sayagues, M.; Vallet-Regi, M.; Hutchison, J.L.; Gonzalez-Calbet, J.M. Modulated structure of  $\text{La}_2\text{NiO}_{4+d}$  as a mechanism of oxygen excess accommodation. *J. Solid State Chem.* **1996**, *125*, 133–139. [[CrossRef](#)]
45. Paulus, W.; Cousson, A.; Dhalenne, G.; Berthon, J.; Revcolevschi, A.; Hosoya, S.; Treutmann, W.; Heger, G.; Le Toquin, R. Neutron diffraction studies of stoichiometric and oxygen intercalated  $\text{La}_2\text{NiO}_4$  single crystals. *Solid State Sci.* **2002**, *4*, 565–573. [[CrossRef](#)]
46. Cleave, A.R.; Kilner, J.A.; Skinner, S.J.; Murphy, S.T.; Grimes, R.W. Atomistic computer simulation of oxygen ion conduction mechanisms in  $\text{La}_2\text{NiO}_4$ . *Solid State Ion.* **2008**, *179*, 823–826. [[CrossRef](#)]
47. Burriel, M.; Garcia, G.; Santiso, J.; Kilner, J.A.; Chater, R.J.; Skinner, S.J. Anisotropic oxygen diffusion properties in epitaxial thin films of  $\text{La}_2\text{NiO}_{4+\delta}$ . *J. Mater. Chem.* **2008**, *18*, 416–422. [[CrossRef](#)]
48. Gauquelin, N.; Weirich, T.; Ceretti, M.; Paulus, W.; Schroeder, M. Long-term structural surface modifications of mixed conducting  $\text{La}_2\text{NiO}_{4+\delta}$  at high temperatures. *Monatsh. Chem. Chem. Mon.* **2009**, *140*, 1095–1102. [[CrossRef](#)]
49. Chroneos, A.; Parfitt, D.; Kilner, J.A.; Grimes, R.W. Anisotropic oxygen diffusion in tetragonal  $\text{La}_2\text{NiO}_{4+\delta}$ : Molecular dynamics calculations. *J. Mater. Chem.* **2010**, *20*, 266–270. [[CrossRef](#)]
50. Garcia, G.; Burriel, M.; Bonanos, N.; Santiso, J. Electrical conductivity and oxygen exchange kinetics of  $\text{La}_2\text{NiO}_{4+\delta}$  thin films grown by chemical vapor deposition. *J. Electrochem. Soc.* **2008**, *155*, 28–32. [[CrossRef](#)]
51. Woolley, R.J.; Illy, B.N.; Ryan, M.P.; Skinner, S.J. In situ determination of the nickel oxidation state in  $\text{La}_2\text{NiO}_{4+\delta}$  and  $\text{La}_4\text{Ni}_3\text{O}_{10-\delta}$  using X-ray absorption near-edge structure. *J. Mater. Chem.* **2011**, *21*, 18592. [[CrossRef](#)]
52. Park, J.C.; Kim, D.K.; Choy, J.H. XAS study on oxygenated  $\text{LaSrNiO}_4$  and  $\text{La}_2\text{NiO}_{4+\delta}$ . *J. Phys. IV* **1997**, *7*, C2-1217–C2-1218.
53. Poccia, N.; Chorro, M.; Ricci, A.; Xu, W.; Marcelli, A.; Campi, G.; Bianconi, A. Percolative superconductivity in  $\text{La}_2\text{CuO}_{4.06}$  by lattice granularity patterns with scanning micro X-ray absorption near edge structure. *Appl. Phys. Lett.* **2014**, *104*, 221903. [[CrossRef](#)]
54. Bianconi, A.; Doniach, S.; Lublin, D. X-ray Ca K-edge of calcium adenosine triphosphate system and of simple Ca compounds. *Chem. Phys. Lett.* **1978**, *59*, 121–124. [[CrossRef](#)]

55. Bianconi, A.; Bachrach, R.Z. Al surface relaxation using surface extended X-ray-absorption fine structure. *Phys. Rev. Lett.* **1979**, *42*, 104–108. [[CrossRef](#)]
56. Bianconi, A. Core excitons and inner well resonances in surface soft X-ray absorption (SSXA) spectra. *Surf. Sci.* **1979**, *89*, 41–50. [[CrossRef](#)]
57. Bianconi, A. Surface X-ray absorption spectroscopy: Surface EXAFS and surface XANES. *Appl. Surf. Sci.* **1980**, *63*, 392–418. [[CrossRef](#)]
58. Della Longa, S.; Soldatov, A.; Pompa, M.; Bianconi, A. Atomic and electronic structure probed by X-ray absorption spectroscopy: Full multiple scattering analysis with the G4XANES package. *Comput. Mater. Sci.* **1995**, *4*, 199–210. [[CrossRef](#)]
59. Bianconi, A. Multiplet splitting of final-state configurations in X-ray-absorption spectrum of metal VO<sub>2</sub>: Effect of core-hole-screening, electron correlation, and metal-insulator transition. *Phys. Rev. B* **1982**, *26*, 2741–2747. [[CrossRef](#)]
60. Bianconi, A.; Congiu-Castellano, A.; De-Santis, M.; Rudolf, P.; Lagarde, P.; Flank, A.M.; Marcelli, A. L<sub>2,3</sub> XANES of the high T<sub>c</sub> superconductor YBa<sub>2</sub>Cu<sub>3</sub>O<sub>~7</sub> with variable oxygen content. *Solid State Commun.* **1987**, *63*, 1009–1013. [[CrossRef](#)]
61. Bianconi, A.; Clozza, A.; Congiu Castellano, A.; Della Longa, S.; De Santis, M.; Di Cicco, A.; Garg, K.B.; Delogu, P.; Gargano, A.; Giorgi, R.; et al. Experimental evidence of itinerant Cu 3d<sup>9</sup>-oxygen hole many body configuration in the high T<sub>c</sub> superconductor YBa<sub>2</sub>Cu<sub>3</sub>O<sub>~7</sub>. *Int. J. Mod. Phys. B* **1987**, *1*, 853–862. [[CrossRef](#)]
62. Bianconi, A.; Desantis, M.; Flank, A.; Fontaine, A.; Lagarde, P.; Marcelli, A.; Katayamayoshida, H.; Kotani, A. Determination of the symmetry of the 3d<sup>9</sup>L states by polarized Cu L<sub>3</sub> XAS spectra of single crystal YBa<sub>2</sub>Cu<sub>3</sub>O<sub>6.9</sub>. *Phys. C Supercond.* **1988**, *153–155*, 1760–1761. [[CrossRef](#)]
63. Bianconi, A.; Campagna, M.; Stizza, S.; Davoli, I. Intermediate valence and near-edge structure in the X-ray absorption spectrum of CePd<sub>3</sub>, γ-Ce, and CeCu<sub>2</sub>Si<sub>2</sub>. *Phys. Rev. B* **1981**, *24*, 6139–6142. [[CrossRef](#)]
64. Bianconi, A.; Marcelli, A.; Dexpert, H.; Karnatak, R.; Kotani, A.; Jo, T.; Petiau, J. Specific intermediate-valence state of insulating 4f compounds detected by L<sub>3</sub> X-ray absorption. *Phys. Rev. B* **1987**, *35*, 806–812. [[CrossRef](#)]
65. Marcelli, A.; Coreno, M.; Stredansky, M.; Xu, W.; Zou, C.; Fan, L.; Chu, W.; Wei, S.; Cossaro, A.; Ricci, A.; et al. Nanoscale phase separation and lattice complexity in VO<sub>2</sub>: The metal-insulator transition investigated by XANES via Auger electron yield at the vanadium L<sub>23</sub>-edge and resonant photoemission. *Condens. Matter* **2017**, *2*, 38. [[CrossRef](#)]
66. Zhou, N.; Chen, G.; Zhang, H.J.; Zhou, C. Synthesis and transport properties of La<sub>2</sub>NiO<sub>4</sub>. *Phys. B Condens. Matter* **2009**, *404*, 4150–4154. [[CrossRef](#)]
67. Dudin, P.; Lacovig, P.; Fava, C.; Nicolini, E.; Bianco, A.; Cautero, G.; Barinov, A. Angle-resolved photoemission spectroscopy and imaging with a submicrometre probe at the spectromicroscopy-3.2L beamline of Elettra. *J. Synchrotron Radiat.* **2010**, *17*, 445–450. [[CrossRef](#)] [[PubMed](#)]
68. Bendele, M.; Barinov, A.; Joseph, B.; Innocenti, D.; Iadecola, A.; Bianconi, A.; Takeya, H.; Mizuguchi, Y.; Takano, Y.; Noji, T.; et al. Spectromicroscopy of electronic phase separation in K<sub>x</sub>Fe<sub>2–y</sub>Se<sub>2</sub> superconductor. *Sci. Rep.* **2014**, *4*, 5592. [[CrossRef](#)] [[PubMed](#)]
69. Jarlborg, T.; Bianconi, A. Electronic structure of superoxygenated La<sub>2</sub>NiO<sub>4</sub> domains with ordered oxygen interstitials. *J. Supercond. Nov. Magn.* **2016**, *29*, 615–621. [[CrossRef](#)]
70. Jarlborg, T.; Bianconi, A. Fermi surface reconstruction of superoxygenated La<sub>2</sub>CuO<sub>4</sub> superconductors with ordered oxygen interstitials. *Phys. Rev. B* **2013**, *87*, 054514. [[CrossRef](#)]
71. Jarlborg, T.; Bianconi, A. Electronic structure of HgBa<sub>2</sub>CuO<sub>4+δ</sub> with self-organized interstitial oxygen wires in the Hg spacer planes. *J. Supercond. Nov. Magn.* **2017**. [[CrossRef](#)]
72. Campi, G.; Bianconi, A. High-Temperature superconductivity in a hyperbolic geometry of complex matter from nanoscale to mesoscopic scale. *J. Supercond. Nov. Magn.* **2016**, *29*, 627–631. [[CrossRef](#)]
73. Campi, G.; Bianconi, A.; Poccia, N.; Bianconi, G.; Barba, L.; Arrighetti, G.; Innocenti, D.; Karpinski, J.; Zhigadlo, N.D.; Kazakov, S.M.; et al. Inhomogeneity of charge-density-wave order and quenched disorder in a high-T<sub>c</sub> superconductor. *Nature* **2015**, *525*, 359–362. [[CrossRef](#)] [[PubMed](#)]
74. Poccia, N.; Ricci, A.; Campi, G.; Bianconi, A. Dislocations as a boundary between charge density wave and oxygen rich phases in a cuprate high temperature superconductor. *Supercond. Sci. Technol.* **2017**, *30*, 035016. [[CrossRef](#)]



75. Campi, G.; Ciasca, G.; Poccia, N.; Ricci, A.; Fratini, M.; Bianconi, A. Controlling photoinduced electron transfer via defects self-organization for novel functional macromolecular systems. *Curr. Protein Pept. Sci.* **2014**, *15*, 394–399. [[CrossRef](#)] [[PubMed](#)]
76. Campi, G.; Di Gioacchino, M.; Poccia, N.; Ricci, A.; Burghammer, M.; Ciasca, G.; Bianconi, A. Nanoscale correlated disorder in out-of-equilibrium myelin ultrastructure. *ACS Nano*. **2018**, *12*, 729–739. [[CrossRef](#)] [[PubMed](#)]



© 2018 by the authors. Licensee MDPI, Basel, Switzerland. This article is an open access article distributed under the terms and conditions of the Creative Commons Attribution (CC BY) license (<http://creativecommons.org/licenses/by/4.0/>).